# Measurement of relative subshell-photoionization cross sections in sodium chloride and sodium fluoride by x-ray-photoelectron spectroscopy

P. C. Kemeny, J. G. Jenkin, J. Liesegang, and R. C. G. Leckey
*Physics Department, La Trobe University, Bundoora, Victoria, Australia 3083*
(Received 21 September 1973)

Relative subshell-photoionization cross sections have been measured directly for solid samples of sodium fluoride and sodium chloride by the technique of x-ray-photoelectron spectroscopy. Values are reported for the subshell-photoionization cross sections of the sodium $2s$ and $2p$; chlorine $2s$, $2p$, $3s$, and $3p$; and fluorine $1s$, $2s$, and $2p$ levels relative to the $1s$ level of sodium. To obtain these values from measured photoelectron line intensities, corrections have been made for (i) the transmission efficiency of the electron energy analyzer, (ii) the angular dependence of the differential subshell-photoionization cross section, and (iii) for the attenuation of the hot electrons as they emerge from a solid sample covered by an adsorbed gas layer, by the use of Auger-electron data acquired simultaneously. Very good agreement is found between the results of the present direct measurements and previous approximate subshell-photoionization cross sections deduced from total-photoionization measurements.

## I. INTRODUCTION

The determination of atomic subshell-photoionization cross sections (SPCS's) has been the subject of both theoretical and experimental research for many years. This sustained interest in SPCS's is due partly to their fundamental importance in the complete description of the photoemission process, and also to their usefulness in other areas such as new methods for quantitative chemical analysis and in particular the quantitative analysis of surfaces.

Some early calculations of SPCS's were performed by Bethe and Salpeter[1] using hydrogenlike atomic wave functions. Since then, total and differential SPCS's have been calculated by numerous authors using more sophisticated wave functions. Recently, Cooper and co-workers[2] have, in a series of papers, calculated the SPCS's of the inert gases, and have also determined the asymmetry parameters $\beta$ of the $s$ and $p$ subshells for many of the elements.

Experimental work in this area has been carried out on the inert gases with a variety of photon energies in the ultraviolet to soft-x-ray range by Siegbahn *et al.*,[3] Krause,[4] and others. A table of the approximate SPCS's for the light elements, at a photon energy of 1486.6 eV (Al $K\alpha$) is contained in a review article by Henke.[5] The values listed therein were obtained indirectly from total-photoelectron-cross-section measurements and theoretical considerations.

In this work we present an evaluation of the use of x-ray-photoelectron-spectroscopy techniques for the determination of relative SPCS's in bulk solids, namely, NaF and NaCl. We define a subshell-photoionization cross section in such a way as to exclude specifically consideration of those processes which leave the ion in other than the ground state (e.g., shake-up or shake-off processes). An examination of our spectra revealed no structure which could positively be identified with such processes, and consequently we consider that the restricted definition given here implies only a small loss of generality. To make these measurements, the technique of x-ray-photoelectron spectroscopy (XPS) has been used to determine the relative intensities of the various photoelectron and Auger-electron lines emitted from a solid sample. The Auger-electron data are used to construct an electron attenuation function (which will be defined and discussed in detail below) for "hot" electrons originating within the solid. This function, which is dependent upon the electron kinetic energy, is used to deduce the relative SPCS's from the remainder of the XPS data. Relative to sodium $1s$, values of the SPCS's of the sodium $2s$ and $2p$; chlorine $2s$, $2p$, $3s$, and $3p$; and fluorine $1s$, $2s$, and $2p$ subshells in sodium chloride and sodium fluoride are reported. Comparisons are then made with the values given by Henke[5] and a number of conclusions are drawn regarding the design of future experiments.

## II. THEORY

It has been shown experimentally and theoretically[2,4,5] that the differential SPCS of the $l$th subshell of the $n$th shell of the $i$th atomic species of a sample is given by

$$\left(\frac{d\sigma}{d\Omega}\right)_{inl} = \sigma_{inl}\,\frac{(1-\frac{1}{2}\beta)+\frac{3}{4}\beta\sin^2\psi}{4\pi}\,, \qquad (1)$$

where $\sigma_{inl}$ is the total SPCS, $\psi$ is the angle between the incoming photon and the outgoing electron, and $\beta$ is the asymmetry parameter which in general can be a function of $i$, $n$, $l$, and the kinetic energy $E$ of

the photoemitted electrons.[2] For convenience we write

$$f(\psi) = [(1 - \tfrac{1}{2}\beta) + \tfrac{3}{4}\beta \sin^2 \psi] \quad . \tag{2}$$

Values of this function for particular $\beta$ values may easily be obtained from Henke.[5]

In order to deduce an expression for the intensity of electrons emitted from the sample in a specific direction, consider the case of a plane semi-infinite solid sample consisting of a homogeneous mixture or compound of various atomic species, irradiated by an extended monochromatic x-ray source (see Fig. 1). The number of photons entering area $dA$ in the angular interval $[\xi, d\xi]$ and $[\eta, d\eta]$ is $\Phi d\xi d\eta dA$, where $\Phi$ is the x-ray flux.

Let the photon mean free path in the material be $\Lambda(E_\gamma)$, where $E_\gamma$ is the photon energy, and let $\lambda(E)$ be the electron mean free path, where $E$ is the kinetic energy of the electron. The number of photoelectrons per second originating from a thin slice of the material parallel to the sample surface, a distance $x$ below the surface, and escaping from the material in the angular region $[\kappa, d\kappa]$ and $[\chi, d\chi]$ is given by

$$dI_{inl} = (\Phi\, d\xi\, d\eta\, dA\, e^{-x/\Lambda\cos\theta})\left[dx N_i \left(\frac{d\sigma}{d\Omega}\right)_{inl} d\Omega\right] \times (e^{(-x/\lambda\cos\phi)}) \quad , \tag{3}$$

where $d\Omega = d\kappa\, d\chi$ and $N_i$ is the atomic density of the $i$th atomic species.

Using the expressions for $(d\sigma/d\Omega)_{inl}$ given by Eqs. (1) and (2), Eq. (3) may be integrated over $x$ to yield

$$dI_{inl} = \frac{\sigma_{inl}}{4\pi} N_i dA \int\int\int\int \Phi f(\psi) \times \frac{\lambda\cos\phi\,\Lambda\cos\theta}{\lambda\cos\phi + \Lambda\cos\theta} d\xi\, d\eta\, d\kappa\, d\chi \quad . \tag{4}$$

Typical values for the electron mean free path $\lambda$ and the photon mean free path $\Lambda$ over the energy ranges of interest are 10 and 10 000 Å, respectively.[5] Therefore, $\Lambda\cos\theta \gg \lambda\cos\phi$ for all but extreme x-ray entry angles; so that, provided the integration is performed over a wide range of angles, the contribution to the integral from those regions where the above approximation breaks down is negligible. Thus, Eq. (4) may be written

$$dI_{inl} = \frac{\lambda\sigma_{inl}}{4\pi} N_i dA \times \int\int\int\int \Phi f(\psi)\cos\phi\, d\xi\, d\eta\, d\kappa\, d\chi \quad . \tag{5}$$

Writing the contribution to Eq. (5) due to angular effects as

$$\Psi_{inl} \equiv \frac{1}{4\pi}\int\int\int\int \Phi f(\psi)\cos\phi\, d\xi\, d\eta\, d\kappa\, d\chi \quad , \tag{6}$$

we obtain the expression for the number of electrons emitted per second in a given direction per unit area of sample as

$$\left(\frac{dI}{dA}\right)_{inl} = \Psi_{inl} N_i \lambda\sigma_{inl} \quad . \tag{7}$$

It should be noted that the quantity $\Psi_{inl}$ is a function of the asymmetry parameter $\beta$ and the experimental geometry only.

A number of effects have been neglected in the development of expression (7) for the intensities of emitted electrons. These include x-ray and electron refraction and reflection at the surface and also the attenuation of electrons due to adsorption of gases onto the surface of the sample. The former effects are negligible provided that x rays enter and electrons leave the surface over a wide range of angles. The latter effect, however, is of considerable consequence in the present work and cannot be neglected. Hence an attenuation factor $e^{-\langle d\rangle/\lambda'}$ is incorporated in the expression (7), where $\langle d\rangle$ is the average distance which an electron will travel through the absorbed gas layer before it escapes into the vacuum, and $\lambda'(E)$ is the mean free path of an electron in the adsorbed layer.

We may now write

$$\left(\frac{dI}{dA}\right)_{inl} = \Psi_{inl} N_i \lambda\sigma_{inl}\, e^{-\langle d\rangle/\lambda'} \quad . \tag{8}$$

In order to use Eq. (8) to extract values of SPCS's

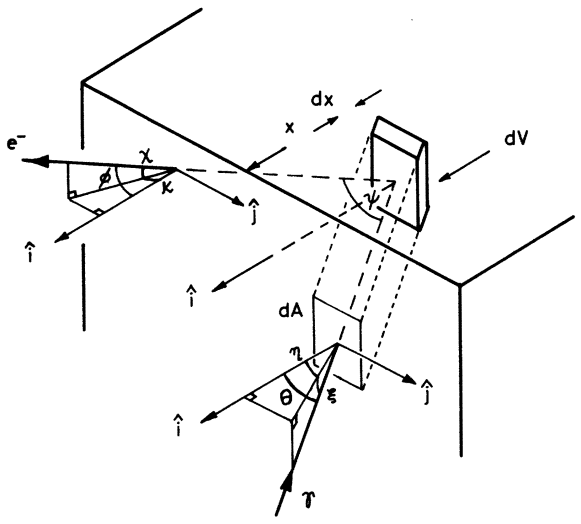


FIG. 1. Segment of a semi-infinite solid sample showing the x rays ($\gamma$) which enter an element of area $dA$ in the direction $(\xi, \eta)$ and the photoelectrons ($e^-$) that are subsequently emitted from an element of volume $dV$ in the direction $(\kappa, \chi)$. See Sec. II of the text, in particular Eq. (3).

from experimental data, the functional forms of the electron mean free paths $\lambda$ and $\lambda'$ must be taken into account. Experiments and theoretical calculations to determine the electron mean free paths in a variety of metallic and nonmetallic materials have been performed over recent years.[6-8] It has been found that the energy-dependent mean free paths for all materials have similar functional energy dependence and differ in magnitude by no more than a factor of 2 or 3 in the energy range of present interest. This functional form may be written[7]

$$\lambda = KE/(\ln E - b) \tag{9}$$

where $K$ and $b$ are constants characteristic of the material.

We now define an electron attenuation function (see Eq. (8))

$$\Gamma(E) = \lambda\, e^{-\langle d\rangle/\lambda'} \tag{10}$$

$$= \frac{KE}{\ln E - b} \exp\left(\frac{-\langle d\rangle(\ln E - b')}{K'E}\right) . \tag{11}$$

From a comparison of the expressions (8) and (7) for the intensities of electron lines from a solid with and without an adsorbed gas layer, and from measurements of electron mean free paths in sodium chloride performed in this laboratory,[8] the quantity $\langle d\rangle$ has been estimated to be approximately 10 Å.

Using this value, expression (11) is plotted in Fig. 2 for some typical values[7] of $K$, $K'$, $b$, and $b'$. It can be seen from the figure that this function is well represented by a straight line over the energy range of interest in this work. Hence

$$\Gamma(E) = \lambda\, e^{-\langle d\rangle/\lambda'} \simeq c(aE - 1) , \tag{12}$$

where $c$ and $a$ are constants. Substituting (12) into (8) we find

$$\left(\frac{dI}{dA}\right)_{inl} = N_i c(aE - 1)\, \sigma_{inl}\, \Psi_{inl} . \tag{13}$$

It is well known that the $K$-shell fluorescence yield of the light elements is extremely small,[9,10] and therefore the only significant channel open for the relaxation of such an ion after the removal of a $K$ electron ($K$-shell photoemission) is the emission of a $KLL$ Auger electron. Thus if $\sigma_{ik}$ is the cross section for production of a particular $KLL$ Auger electron from the $i$th atomic species, then the total photoionization cross section for the 1$s$ level of the $i$th atomic species is

$$\sigma_i(1s) = \sum_k \sigma_{ik} , \tag{14}$$

that is, for the $i$th atomic species the total 1$s$ photoelectron yield from the volume element $dV$ is taken to be equal to the sum of all of the $KLL$ Auger yields. Since Eq. (13) also provides a valid description for Auger-electron intensities it may be used to provide expressions for both $\sigma_i(1s)$ and $\sigma_{ik}$, and hence from Eq. (14) we have

$$\frac{1}{\Psi_i(1s)[aE_i(1s) - 1]}\left(\frac{dI(1s)}{dA}\right)_i = \sum_k \frac{1}{\Psi_{ik}(aE_{ik} - 1)}\left(\frac{dI}{dA}\right)_{ik} , \tag{15}$$

where $E_i(1s)$ is the kinetic energy of the 1$s$ photoelectron from the $i$th atomic species and $E_{ik}$ is the energy of a particular $KLL$ Auger electron from

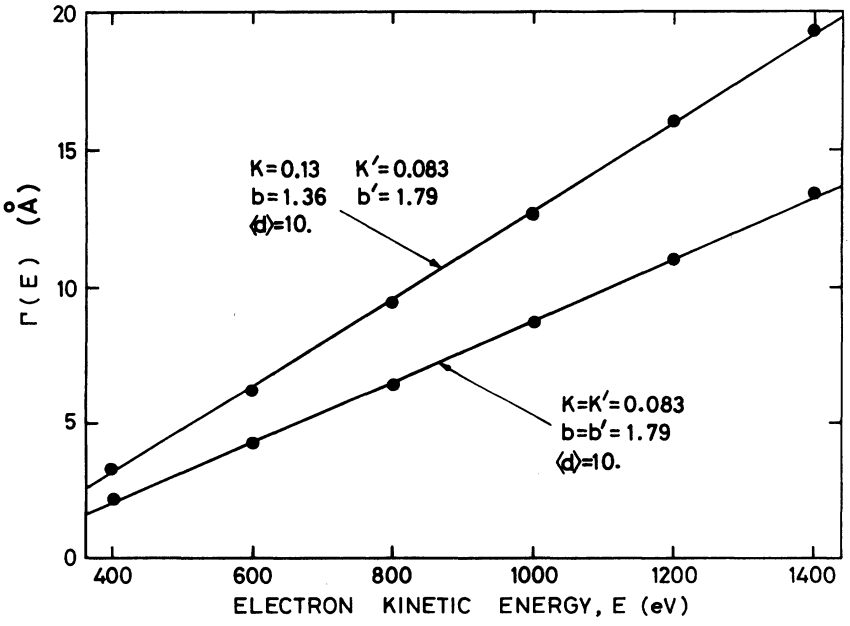


FIG. 2. Electron attenuation function $\Gamma(E)$ [Eq. (11)] plotted as a function of electron kinetic energy for some typical values of the parameters $K$, $K'$, $b$, $b'$ (Ref. 7); $\langle d\rangle$ is the average distance that an electron travels through an adsorbed gas layer. A linear relationship may be seen to exist over the energy range of interest (see Sec. II, Eq. (12)].

the $i$th atomic species. The quantities $(dI(1s)/dA)_i$, $(dI/dA)_{ik}$, $E_i(1s)$, and $E_{ik}$ are obtained from the XPS data. $\Psi_i(1s)$ and $\Psi_{ik}$ can be calculated from the geometry of the instrument and a knowledge of the asymmetry parameter $\beta$. For $s$ electrons, $\beta = 2$,[2,5] while $KLL$ Auger emission is isotropic,[7] whence $\beta = 0$.

Thus Eq. (15) may be solved for $a$, the parameter used to define the linear electron attenuation function $\Gamma(E)$ in Eq. (12). Equation (13) and the value of $a$ so obtained are then used to find the SPCS's relative to the sodium 1$s$ line.

In order to find the $p$-subshell cross sections from Eq. (13), $\Psi_i(np)$ must be evaluated. Although $\beta$ is not accurately known for these subshells at the photon energy used, typical values of $\beta$ are in the range 1.0–1.5.[5] In order to estimate $p$-shell SPCS's, $\Psi_i(np)$ has been evaluated using $\beta = 1.3$. This choice is consistent with the recent work of Manson.[2]

A number of possible sources of error in the method presented above for the determination of $\Gamma(E)$ and subsequently of SPCS's are readily identifiable. Of these the production of $K$-shell vacancies by bremsstrahlung generated in the x-ray source must be carefully considered. We have treated this effect in some detail in the Appendix and have estimated that it produces an intrinsic error of approximately 5% in the measured SPCS values given in the present work. In addition, this effect is likely to be partially cancelled by our neglect of the fluorescence decay channel in the relaxation of an ionized Na or F atom. Another likely source of error in the present determinations is represented by the possibility of $K$-shell ionization by "hot" photoelectrons. The contribution to the total Auger emission from such events has been estimated from the SPCS's of Henke,[5] the electron-ionization cross sections of Pessa and Newell[11] and from Eq. (7). It is found that this phenomenon contributes less than 1 part in $10^5$ of the total emission of Auger electrons from the sample.

The inclusion of the angular asymmetry terms in our treatment is strictly valid for free atoms. In a solid, subsequent elastic collisions involving the ionic potential wells may conceivably affect the angular distribution of photoelectrons from a particular shell; but we consider that this effect is negligible because (a) the number of elastic collisions made by such an electron prior to escape from the sample or prior to an inelastic encounter is small[5,12] and (b) a common feature of all elastic scattering theories (e.g., screened Coulomb scattering) is the predominance of small-angle events.[13]

## III. EXPERIMENTAL

The apparatus used in this experiment has been described in detail elsewhere.[14,15] Basically, it consists of a 90° sector, spherical electrostatic electron energy analyzer with a cylindrical Al $K\alpha$ (1486.6-eV) soft-x-ray source. The system is pumped by a 1200-liter/sec, liquid-nitrogen-trapped oil diffusion pump and the working pressure is $5\times10^{-7}$ torr. Photoelectron spectra are accumulated in a 1024-channel multichannel analyzer by holding the analyzer at a fixed pass energy and varying the accelerating/retarding potential in synchronization with the channel-advance clock of the multiscaler.[14]

Samples are prepared by evaporation from a tungsten boat onto a rotating polished-aluminium cylindrical substrate. Sample thickness ($\sim10^3$ Å) was monitored by an Ultec model No 60-915 deposit-thickness monitor. This preparation procedure ensures that the sample thickness is large compared to the electron mean free path. Upon completion of evaporation, the sample can be immediately lowered into the normal operating position without its removal from the vacuum system. Values of the angular-dependent functions $\Psi_{inl}$ as calculated for the present geometry[15] are listed in Table I.

Because the region from which photoelectrons are emitted is extremely thin ($\sim$30 Å) compared with the radius of curvature of the sample rod ($\sim$0.3 cm), the theoretical analysis of Sec. II, developed for a flat sample, may be applied.

Due primarily to contamination of the x-ray anode, the x-ray intensity varies with time. It is also apparent[16] that the rate of growth of adsorbed gas layers is approximately of the form $d(1-e^{-t/\tau})$, where $d$ is the asymptotic limit of the gas layer thickness and $\tau$ is a time constant no greater than a few seconds at the pressure used for this experiment ($5\times10^{-7}$ torr). From these considerations it is clear that the measured intensities of the various photoelectron and Auger peaks are time dependent. Therefore spectra were recorded by alternating rapidly between acquisition of the sodium 1$s$ line and acquisition of the line under investigation. Each spectrum represents at least 200 individual scans over the energy range of interest, and typically the number of counts acquired per channel was several thousand. The sodium 1$s$ line was used as the reference level for all relative intensity measurements.

TABLE I. Values of the angular distribution function $\Psi_{inl}$ for Auger electrons and $s$- and $p$-subshell photoelectrons [see Eq. (16)].

| Origin of electron | $\beta$ | $\Psi_{inl}$ |
|---|---|---|
| $s$ subshell | 2 | 0.111 |
| $p$ subshell | 1.3 | 0.095 |
| Auger | 0 | 0.080 |

## IV. RESULTS

Figure 3 shows two typical spectra from sodium fluoride, Fig. 3(a) being the photoelectron spectrum of the sodium 1*s* level and Fig. 3(b) the sodium *KLL* Auger lines. Assignment of the peaks in Fig. 3(b) is due to Siegbahn *et al.*[10] The sodium chloride photoelectron and Auger spectra contain similar features.

It is clear from Figs. 3(a) and 3(b) that there is some structure on the low kinetic energy side of both the sodium 1*s* photoelectron and sodium Auger lines in the sodium fluoride electron spectra in addition to the usual, slowly increasing inelastic scattered background. The sodium 1*s* spectrum was smoothed by a nine-point-polynomial smoothing procedure, and the resultant spectrum corrected for the transmission efficiency of the analyzer. The results of this procedure which is shown in Fig. 4(a) clearly reveals a small peak 11.7(5) eV below the center of the primary line, and an elevated smooth background extending some distance below

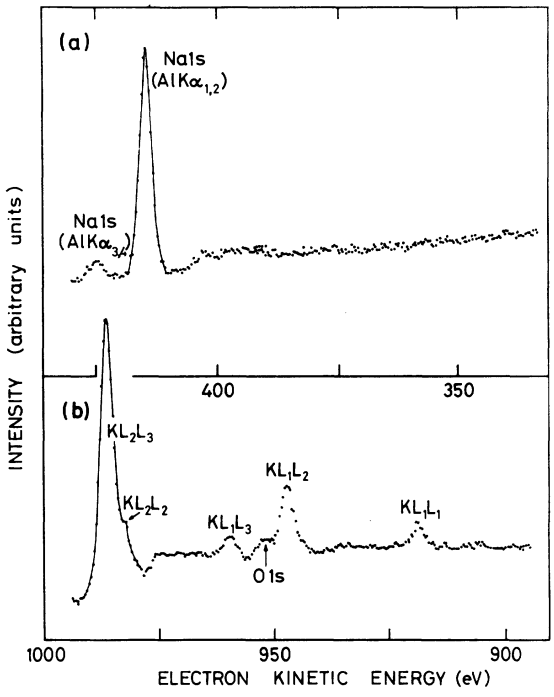


FIG. 3. Typical spectra from the present work: (a) the sodium 1*s* photoelectron peak from sodium fluoride. On the high kinetic energy side of this line is a smaller peak due to Al $K\alpha_{3,4}$ x-ray satellited while on the low kinetic energy side there is a well defined structure whose origin is discussed in the text. (b) The *KLL* Auger spectrum of sodium from sodium fluoride. The various features of this spectrum are assigned according to Siegbahn (Ref. 10). A well-defined shoulder, similar to that in Fig. 3(a), may be seen on the low kinetic energy side of the $KL_2L_3$ Auger line.

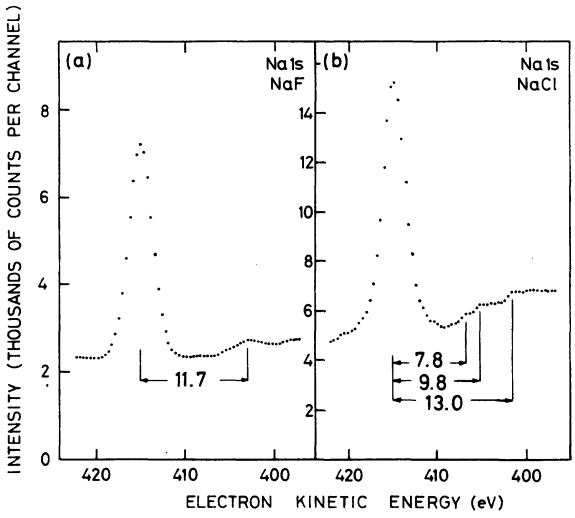


FIG. 4. Sodium 1*s* photoelectron lines from (a) sodium fluoride and (b) sodium chloride. Both spectra have been smoothed by a nine-point polynomial smoothing procedure and corrected for the transmission efficiency of the analyzer. The significance of the energy separations of the features in these spectra is discussed in the text.

this peak. A number of possible inelastic scattering processes were considered in seeking an explanation for this feature; for example, (i) electron-exciton scattering, which would yield some structure approximately 10.7 eV below the principal line[17] and (ii) electron-ionization scattering, a process consistent with the observed features; namely, the onset edge or threshold on the low-energy side of each observed line together with a wide inelastic electron distribution corresponding to the excitation of electrons from the 2*p* valence band of the fluoride anion into a wide conduction band beginning near the vacuum level (see Fig. 3). The binding energy of the $F^-$ 2*p* band in sodium fluoride with respect to the vacuum level has recently been measured as 11.88(10) eV,[18] and this agrees well with the separation of 11.7(5) eV from Fig. 4(a). This interpretation is also consistent with the recent work of Battye *et al.*[19] which shows that ionization involving valence-band electrons is the dominant electron energy loss mechanism in insulators.

A portion of the electron spectrum from NaCl in the region of the Na 1*s* photoelectron peak, after smoothing and correcting for the transmission efficiency of the analyzer, is shown in Fig. 4(b). The structure apparent on the low-energy side of the main line is more complex and less pronounced than for NaF, but was consistently reproduced in NaCl spectra taken on several occasions. The weak maxima at 7.8(5) and 9.8(5) eV below the center of the photopeak are consistent with the 8.0-eV exciton doublet and 10-eV maximum seen in the optical

absorption spectrum of NaCl.[17] The structure at 9.8(5) eV below the photopeak may be associated with ionization from the $Cl^-$ $2p$ valence band which is located 10.45(10) eV below the vacuum level.[20] The origin of the shoulder at approximately 13.0(5) eV below the photopeak has not been determined. These various energy-loss processes no doubt provide an important contribution to the electron mean free path discussed earlier.

Before a detailed analysis of the spectra can be made it is necessary to correct for the transmission efficiency of the spectrometer. In a previous work[14] an expression was developed for the calculation of the true peak intensity of a photoelectron distribution from the measured peak intensity. For the present situation, Eq. (15) of Ref. 14 can be written

$$I_{0\ \mathrm{peak}} = \frac{CN\Delta E E_0^2}{E'_{k0}\,(E_0^2 + R^2\Delta E^2)^{1/2}} \quad , \tag{16}$$

where $I_{0\ \mathrm{peak}}$ is the measured peak height of a photoelectron line, $N$ is the true peak height, $\Delta E$ is the full width at half-maximum (FWHM) of the true peak, $E_0$ is the pass energy of the energy analyzing element of the spectrometer, $E'_{k0}$ is the kinetic energy of the photoelectrons before retardation, $C$ is a constant of the instrument, and $R$ is the resolving power defined by

$$R = E_0/\Delta E_0 \quad . \tag{17}$$

For Gaussian line shapes it is well known that

$$\Delta E_m^2 = \Delta E_0^2 + \Delta E^2 \quad , \tag{18}$$

where $\Delta E_m$ is the FWHM of the measured photoelectron intensity distribution.

Substituting for $R$ and $\Delta E$ from Eqs. (17) and (18) into Eq. (16) gives

$$I_{0\ \mathrm{peak}} = \frac{C}{R}\,\frac{(N\Delta E)}{\Delta E_m}\,\frac{E_0^2}{E'_{k0}} \quad .$$

Multiplying through by $\Delta E_m$ and interpreting the quantities $(I_{0\ \mathrm{peak}}\Delta E_m)$ and $(N\Delta E)$ as being proportional to the areas $A_m$ and $A$ under the measured and true photoelectron peaks, respectively, we can write

$$A_m = C'A E_0^2/E'_{k0} \quad . \tag{19}$$

After subtraction of background, Eq. (19) may be used to compare the intensities of photoelectron and Auger lines of various energies. The present data and their corrections for the effects discussed in Secs. 2–4 are summarized in Tables II and III for sodium fluoride and sodium chloride, respectively. The first four columns of Tables II and III list, respectively, the various photoelectron and Auger lines, their approximate kinetic energies, the number of counts in the peaks relative to the sodium 1$s$ photoelectron line, and the intensities of these peaks corrected for the transmission efficiency of the analyzer.

Because the binding energies of the sodium 2$p$ and fluorine 2$s$ levels are very similar, only the sum of the intensities of the corresponding photo-

TABLE II. Summary of experimental results for sodium fluoride. Column 6 contains the measured relative SPCS values (±10%) for the various subshell photoelectrons and Auger electrons. The data shown in other columns are explained in the text.

| Electron line | Electron kinetic energy (eV) | Measured line intensity | Transmission efficiency corrected line intensity | Angular distribution corrected line intensity | Attenuation function corrected line intensities (relative SPCS) | Relative SPCS according to Henke (Ref. 5) |
|---|---|---|---|---|---|---|
| Na $1s_{1/2}$ | 415 | 1.0 | 1.0 | 1.0 | 1.0 | 1.0 |
| Na $2s_{1/2}$ | 1424 | 0.057 | 0.20 | 0.20 | 0.053 | 0.051 ($t$) |
| Na $KL_1L_1$ | 920 | 0.037 | 0.082 | 0.12 | 0.049 | |
| Na $KL_1L_2$ | 947 | 0.98 | 0.22 | 0.31 | 0.13 | |
| Na $KL_1L_3$ | 959 | 0.042 | 0.097 | 0.14 | 0.055 | |
| Na $KL_2L_2$ / $KL_2L_3$ | 987 | 0.58 | 1.39 | 1.94 | 0.77 | |
| F $1s_{1/2}$ | 801 | 0.58 | 1.11 | 1.11 | 0.55 | 0.52 ($t$) |
| F $2s_{1/2}$ + Na $2p_{1/2,3/2}$ | 1456 | 0.092 | 0.22 + (0.10) | 0.22 + (0.027) | 0.057 + (0.032) | 0.022 ($g$) + (0.017) ($t$) |
| F $2p_{1/2,3/2}$ | 1478 | $6.7\times10^{-3}$ | 0.024 | 0.028 | $7.3\times10^{-3}$ | $7.2\times10^{-3}$ ($g$) |
| F $KL_1L_1$ | 610 | 0.026 | 0.038 | 0.053 | 0.035 | |
| F $KL_1L_2$ | 628 | 0.063 | 0.095 | 0.13 | 0.085 | |
| F $KL_1L_3$ | 636 | 0.027 | 0.042 | 0.059 | 0.037 | |
| F $KL_2L_2$ / $KL_2L_3$ | 654 | 0.30 | 0.48 | 0.67 | 0.405 | |

TABLE III. Summary of experimental results for sodium chloride. Column 6 contains the measured relative SPCS values (±10%) for the various subshell photoelectrons and Auger electrons. Only those sodium *KLL* Auger lines which were observed in the present experiment are listed. The data shown in other columns are explained in the text.

| Electron line | Electron kinetic energy (eV) | Measured line intensity | Transmission efficiency corrected line intensity | Angular distribution corrected line intensity | Attenuation function corrected line intensities (relative SPCS) | Relative SPCS according to Henke (Ref. 5) |
|---|---|---|---|---|---|---|
| Na $1s_{1/2}$ | 415 | 1.0 | 1.0 | 1.0 | 1.0 | 1.0 |
| Na $2s_{1/2}$ | 1424 | 0.055 | 0.19 | 0.19 | 0.052 | 0.051($t$) |
| Na $2p_{1/2,3/2}$ | 1456 | 0.029 | 0.10 | 0.12 | 0.032 | 0.017($t$) |
| Na $KL_1L_2$ | 947 | 0.10 | 0.23 | 0.32 | 0.13 | |
| Na $KL_1L_3$ | 959 | 0.052 | 0.12 | 0.17 | 0.068 | |
| Na $KL_2L_3$ / $KL_2L_2$ | 987 | 0.61 | 1.45 | 2.02 | 0.80 | |
| Cl $2s_{1/2}$ | 1217 | 0.19 | 0.55 | 0.55 | 0.18 | 0.24($t$) |
| Cl $2p_{1/2,3/2}$ | 1286 | 0.30 | 0.94 | 1.10 | 0.33 | 0.23($t$) |
| Cl $3s_{1/2}$ | 1469 | 0.012 | 0.042 | 0.042 | 0.011 | |
| Cl $3p_{1/2,3/2}$ | 1480 | 0.027 | 0.095 | 0.11 | 0.029 | |

electron lines can be measured in the present experiment. The result of the measurement for these overlapping levels is shown in the row labeled "F $2s$ + Na $2p$" of Table II. However, the sodium $2p$ SPCS relative to that of the sodium $1s$ level is known approximately from the present sodium chloride results (Table III). Therefore, the relative contributions to the measured intensity from the two levels, sodium $2p$ and fluorine $2s$, can be estimated. The results are shown in column 4 of Table II. The number in parentheses is the Na $2p$ contribution from column 4 of Table III, while the other figure is the contribution of fluorine $2s$ relative to the sodium $1s$ level.

It is to be noted that the dominant Al-$K\alpha_{1,2}$ x-ray line (itself an unresolved doublet) has several weaker satellites. These lines give rise to additional holes in the $1s$ shells of the sodium and fluorine ions of the solids. The resulting photoelectrons are clearly separated in the spectra [Fig. 3(a)] from the main photoelectron lines, but no such spectral separation occurs for the Auger lines. The measured intensities of the latter are therefore corrected by subtraction of the satellite photoelectron intensities. This correction (approximately 10% in the present case) has already been made to the Auger intensities listed in the third columns of Tables II and III.

These results must further be corrected for the angular-distribution effect and electron-attenuation function discussed in Sec. II. The former correction is obtained using Table I and the resulting relative yields are listed in the fifth columns of Tables II and III. The sodium Auger-electron data have been used to determine the electron attenuation function in conjunction with Eq. (15) for the sodium fluoride and sodium chloride samples. The sum of the corrected sodium Auger intensities in column 6 of the tables is therefore constrained to be 1.0; i.e., equal to the Na $1s$ intensity. No such constraint has been applied to the fluoride Auger intensities. These and all the photoelectron intensities have been corrected for electron attenuation using Eq. (13) and are listed in column 6 of the tables. The adequacy and self-consistency of the present method is demonstrated by the close agreement between the sum of the relative fluorine Auger intensities (0.56) and the relative fluorine $1s$ photoelectron intensity (0.55). The relative intensities listed in column 6 of the tables are equal to the subshell photoionization cross sections relative to the sodium $1s$ SPCS.

## V. DISCUSSION

The results of the present work are shown in Tables II and III. The Auger data have been discussed in Secs. I–IV, but a number of points are now made concerning the photoelectron data.

First, the consistency of the SPCS of the sodium $2s$ level as measured from the two samples, sodium fluoride and sodium chloride, is very satisfactory (column 6 of Tables II and III).

The present results for SPCS's relative to the sodium $1s$ level may be compared with those of Henke,[5] where available, as listed in column 7 of Tables II and III. The postscript letters $t$ and $g$ refer to values taken from the tables and graphs, respectively, of Ref. 5. This is necessary because the tables do not extend over the range of atomic number required here, while the graphs do. If one

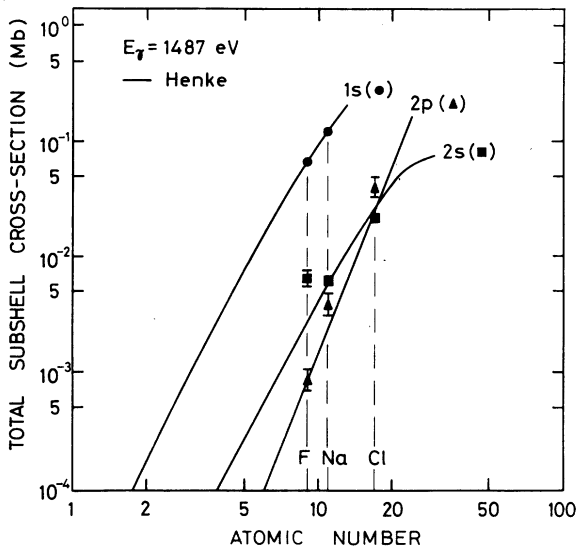


FIG. 5. Subshell photoionization cross sections, as measured in the present work, plotted as a function of atomic number. Henke's value for the SPCS of the sodium 1*s* level (Ref. 5) is used to provide a calibration in absolute units. The solid lines, derived from total photoionization cross-section measurements, are due to the same author.

accepts the value of Henke for the absolute SPCS of sodium 1*s* the results of the present work may be plotted in absolute units of cross section as a function of atomic number. Comparison between the present work and that of Henke[5] may be made by reference to Tables II and III and to Fig. 5. The SPCS values given by Henke were obtained indirectly from total photoabsorption cross-section measurements and certain theoretical arguments. The over-all agreement is excellent for the *s* subshell photoionization cross sections. A small disparity exists, however, between the values of the *p* subshell SPCS's. In particular, the discrepancies in the sodium and chlorine 2*p* results exceed the expected uncertainties of this experiment. It is hoped that future experiments will reveal the source of these discrepancies.

## VI. CONCLUSION

The internal consistency, and good over-all agreement of the present measurements of SPCS's in sodium fluoride and sodium chloride with previous indirectly obtained results demonstrate the usefulness of the technique of photoelectron spectroscopy for the measurement of individual SPCS's in bulk solids.

Future experiments can, however, be improved in a number of respects. Of major importance is the use of an ultrahigh vacuum system which will simplify the interpretation procedure since the formation of adsorbed gas layers can greatly be reduced. Similarly, an instrument in which the incident x-ray and emergent electron beams are more highly collimated would facilitate the interpretation of data provided that various angular parameters are carefully chosen.[5] In addition, improved techniques for the measurement of electron mean free paths are currently being utilized.[9] These techniques could be applied concurrently with SPC experiments, obviating the necessity for such heavy reliance of Auger data for the determination of electron attenuation. In fact Auger-line intensities could be misleading in this respect for SPCS measurements made at higher photon energies (e.g., using Cu-$K\alpha$ or Cr-$K\alpha$ photons) unless an x-ray source with crystal monochromator was used. This is because of the rapid increase, with incident electron energy and anode atomic number, of the ratio: bremsstrahlung-to-characteristic radiation—see Appendix and also Eq. (15.27) of Ref. 21. Nevertheless, Auger data, if interpreted with caution, do provide a useful check on direct mean free path information.

Under the experimental conditions described above, a wide range of materials should be susceptible to SPCS measurements. It is hoped that the availability of new SPCS information will generate interest in the theoretical calculation of SPCS's for solids, particularly in the soft x-ray region. Calculation of the SPCS's for the outermost electron energy bands would be particularly interesting since it is to be expected that solid-state effects are most readily observable for these levels.

## APPENDIX

We consider here the possibility that bremsstrahlung produced by the 6-kV x-ray source could cause significant production of *K*-shell vacancies in the sample leading not only to the generation of photoelectrons of energies other than that associated with Al $K\alpha$ radiation, but also to the generation of Auger electrons indistinguishable from those produced by Al $K\alpha$ radiation.

Bremsstrahlung as produced by the source is known to be distributed in energy according to the Bethe-Heitler formula[21] to a good approximation, but the radiation reaching the sample is strongly attenuated by a 9-$\mu$m Al-foil filter incorporated in the present source for energies in the range 1.5–3.0 keV.[15] In addition the production of *K*-shell photoelectrons by high-energy bremsstrahlung is limited by the *K*-shell photoionization cross section, which has a similar functional dependence with energy for Na and Fl,[22] in that it decreases sharply for photon energies above ~1 keV.

The Al filter does not attenuate bremsstrahlung significantly for energies in the region 600–1500

eV and consequently it is necessary to determine the contribution of $K$-shell ionization made by this radiation. In order to calculate the intensity of Al $K\alpha$ radiation at the sample we have used the semiempirical formulas and experimental data given by Pessa and Newell[11] for the $K$-shell electron impact ionization cross section of Al, in conjunction with the fluorescence yield given by Bambynek *et al.*[23] Numerical integration of the Bethe-Heitler expression for bremsstrahlung production, after modification to account for the effects of the x-ray filter and for the variation of $K$-shell photoionization cross section,[22] has been performed. In this manner we have estimated that the ratio of the number of (for example) Na $K$-series Auger electrons produced by bremsstrahlung to the number produced by Al-$K\alpha$ radiation is close to 5%. We might therefore expect to observe an additional 5% of Na ($KLL$) Auger electrons were it not for our assumption that the fluorescence yield of Na is zero. In fact the Na fluorescent yield is likely to be ~1 or 2%[23] leading to a reduction in the production of Auger electrons following $K$-shell ionization. This effect partially offsets the additional Auger production by bremsstrahlung as discussed above.

The estimate given here for the relative unimportance of bremsstrahlung is supported by a statement by Birks[24] who remarks that for elements with $Z \approx 14$ (Si) the ratio (characteristic-radiation to bremsstrahlung) is in excess of $10^4$ in the neighborhood of the dominant characteristic x-ray line.


[1]H. A. Bethe and E. Salpeter, in *Quantum Mechanics of One- and Two-Electron Atoms* (Academic, New York, 1957).

[2]J. Cooper and R. N. Zare, J. Chem. Phys. 48, 942 (1968); J. W. Cooper and S. T. Manson, Phys. Rev. 177, 157 (1969); D. J. Kennedy and S. T. Manson, Phys. Rev. A 5, 227 (1972); S. T. Manson and J. W. Cooper, Phys. Rev. 165, 126 (1968); J. Cooper, Phys. Rev. 128, 681 (1962); S. T. Manson, Phys. Rev. Lett. 26, 219 (1971); S. T. Manson, J. Electron Spectrosc. 1, 413 (1972).

[3]K. Siegbahn, C. Nordling, G. Johansson, J. Hedman, P. F. Heden, K. Hamrin, U. Gelius, T. Bergmark, L. O. Werme, R. Manne, and Y. Baer, in *E.S.C.A. Applied to Free Molecules* (North-Holland, Amsterdam and London, 1969), p. 23–46.

[4]M. O. Krause, Phys. Rev. 177, 151 (1969); Phys. Rev. 140, A1845 (1965); M. O. Krause and T. A. Carlson, Phys. Rev. 149, 52 (1966); F. Wuilleumier and M. O. Krause, in *Electron Spectroscopy*, edited by D. A. Shirley (North-Holland, Amsterdam, 1972).

[5]B. L. Henke, U. S. Air Force Office of Scientific Research Technical Report No. AFOSR-TR-72-1140 (1972).

[6]J. Tejeda, M. Cardona, N. J. Shevchick, D. W. Langer, and E. Schönherr, Phys. Status Solidi B 58, 189 (1973).

[7]E. Bauer, Vacuum 22, 539 (1972).

[8]F. L. Battye, J. Liesegang, R. C. G. Leckey, and J. G. Jenkin (unpublished).

[9]See, for example, R. Schaeffer, J. Appl. Phys. 44, 152 (1973).

[10]K. Siegbahn, C. Nordling, A. Fahlman, R. Nordberg, K. Hamrin, J. Hedman, G. Johansson, T. Bergmark, S. Karlsson, I. Lindgren, and B. Lindberg, Nova Acta Reg. Soc. Sci. Upsaliensis 20, 1 (1967).

[11]V. M. Pessa and W. R. Newell, Physica Scripta 3, 165 (1971).

[12]E. J. Sternglass, Phys. Rev. 95, 345 (1954).

[13]N. F. Mott and H. S. W. Massey, *The Theory of Atomic Collisions*, 3rd ed. (Clarendon, Oxford, 1965), p. 235.

[14]P. C. Kemeny, A. D. McLachlan, F. L. Battye, R. T. Poole, R. C. G. Leckey, J. Liesegang, and J. G. Jenkin, Rev. Sci. Instrum. 44, 1197 (1973).

[15]A. D. McLachlan, R. C. G. Leckey, J. G. Jenkin, and J. Liesegang, Rev. Sci. Instrum. 44, 873 (1973).

[16]A. D. McLachlan, J. Liesegang, R. C. G. Leckey, and J. G. Jenkin, J. Electron Spectrosc. 3, 207 (1974).

[17]C. Kittel, in *Introduction to Solid State Physics*, 3rd ed. (Wiley, New York, 1967), p. 545.

[18]R. T. Poole, J. Liesegang, R. C. G. Leckey, and J. G. Jenkin, Chem. Phys. Lett. 23, 194 (1973).

[19]F. L. Battye, J. Liesegang, J. G. Jenkin, and R. C. G. Leckey, Phys. Rev. B (to be published).

[20]R. T. Poole, J. G. Jenkin, R. C. G. Leckey, and J. Liesegang, Chem. Phys. Lett. 22, 101 (1973).

[21]J. D. Jackson, *Classical Electrodynamics* (Wiley, New York, 1962) p. 509–519.

[22]B. L. Henke and R. L. Elgin, Adv. X-Ray Analysis 13, 639 (1970).

[23]W. Bambynek, B. Crasemann, R. W. Fink, H. U. Freund, H. Mark, R. E. Price, P. V. Rao, and C.D. Swift, Rev. Mod. Phys. 44, 717 (1972).

[24]L. S. Birks, *Electron Probe Microanalysis* (Interscience, New York, 1963), p. 63.